MODEL-BASED ANALYSIS OF SENSOR-NOISE IN PREDICTIVE PASSIVE SAFETY ALGORITHMS

Tobias Dirndorfer
Robotics and Embedded Systems, Technische Universität München
Michael Botsch
Department for Active and Passive Safety, AUDI AG, Ingolstadt
Alois Knoll
Robotics and Embedded Systems, Technische Universität München
Germany
Paper Number 11-0251

ABSTRACT

The introduction of environment perception sensors into the automotive world enables further improvement of the already highly optimized passive safety systems. Such sensors facilitate the development of safety applications that can act in a context sensitive manner concerning the protection of vehicle occupants. Hereby the quality of the provided information is decisive for the usability and effective range of such sensors within integrated safety systems. In this paper noise effects in sensors and their implications on the prediction of collision parameters are analyzed. The focus lies on sensors that can measure distances but not velocities or accelerations of the objects surrounding the car. For such sensors a noise model is presented as well as a tracking algorithm aiming to estimate the velocities and to compensate the effects of noise. This information is used by a trajectory-based algorithm to predict relevant collision parameters like time-to-collision, relative velocity at collision time etc. Monte Carlo simulations show the influence of noise on the accuracy of the predicted collision parameters. The described model-based study allows the systematic deduction of sensor requirements and represents a new way for the evaluation of the robustness of predictive passive safety systems.

INTRODUCTION

Modern cars provide a high level of safety due to the optimization of bodywork, seat-belts or airbags in the last decades. Conventional passive safety applications for the activation of occupant restraint systems work on established sensor concepts, e.g., acceleration and pressure sensors, and have already reached a high level of adaptivity and robustness. The introduction of environment perception sensors leads to a further improvement of security, since safety systems can be developed that act in a context sensitive manner [1, 2, 3, 4]. First applications like the proactive reversible belt-tensioner can already be found in new cars, e. g., in the Audi A7 [5], and the adaptation of airbags and other passive safety systems to the specific crash situation are in the focus of current development. Future cars will combine all available information—including those gained by Car-to-X (http://www.simTD.de, http://www.car-to-car.org) technologies—concerning the environment to increase the effectiveness of vehicle safety in an integral sense.

The number of sensors that are and will be integrated in new vehicles is increasing since applications have various requirements concerning the range, aperture, sensitivity or other properties. Typical applications using such sensors are mainly located in the field of advanced driver assistance systems like automatic cruise control, lane assist, heading control, etc. In the vehicle safety domain requirements on such sensors are high, i. e., a very small false positive rate and a very high true positive rate in the detection of objects in the environment of the car. Not only the detection of an object's existence is of high interest but also its exact location, velocity and geometry. Such pre-crash information allows the estimation of collision parameters before a collision occurs. This information can be used to optimize the activation of adaptive restraint systems. However, the pre-crash-prediction of the collision parameters is subject to a couple of disturbance effects, e.g., inexact measurements as well as time delays caused by tracking algorithms or the communication between different electronic control units. These factors can affect

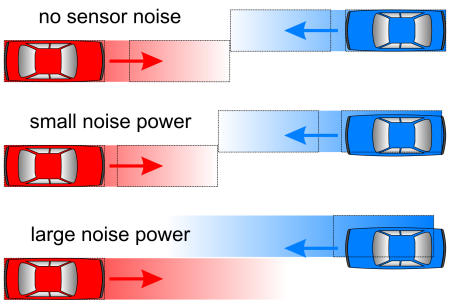

Figure 1. Effects of sensor noise on the collision prediction

the required precision of predictive crash severity estimations and therefore the effectiveness of integrated safety systems. The example from Figure 1 illustrates that a large noise power of the predictive sensor can lead to a wrong prediction of how a scenario will develop in the future. Assuming that the dynamic parameters like velocities or accelerations do not change during the prediction interval a small noise power disturbs the prediction marginally, whereas a large noise power can lead to a completely wrong estimation of the scenario. The first illustration in Figure 1 shows a prediction with no measurement noise, the second illustration the same scenario but under the assumption that small noise power disturbs the measurement and the third illustration the same scenario but under the assumption that a large noise power disturbs the measurement. Therefore, it is necessary to quantify the effect of noise on predictions that are used to adapt restraint systems by taking into account the whole signal processing chain. This paper focuses on such a model of disturbance effects and their influence on the computation of relevant collision parameters like the time-to-collision, the relative velocity at collision time, the collision angle and further geometric parameters. On the one hand the noise caused by sensors describing the state of the ego vehicle and on the other hand the noise caused by predictive sensors detecting the vehicle environment are considered. Whereas a stationary white noise Gaussian random process is assumed for the noise disturbing the ego-state, for the predictive sensor a more sophisticated model is applied. The focus lies on sensors able to measure the position and geometry of objects but not their velocity and acceleration. The velocity must be estimated based on position changes which is accomplished here using a Kalman filter. Thus, the noise process describing the inaccuracy of the position measurement determines the noise process for the velocity. The model for position inaccuracies takes into account a distance based noise power. On the basis of such a noise model Monte Carlo simulations are performed for four predictive sensor variants to analyze the effects on the computed collision parameters. The four sensor variants were chosen to represent sensors with different performances.

The chapter "MEASUREMENT DATA" introduces the relative dynamics model and the sensor noise model that are used in the Monte Carlo simulations later on. Chapter "COLLISISION PREDICTION ALGORITHM" focuses on the tracking model and on the trajectory-based prediction module used to calculate the collision parameters. In Chapter "MONTE CARLO SIMULATION" three traffic scenarios are analyzed in detail and the effects of noisy measurements are presented. The general outline of the paper is illustrated in Figure 2.

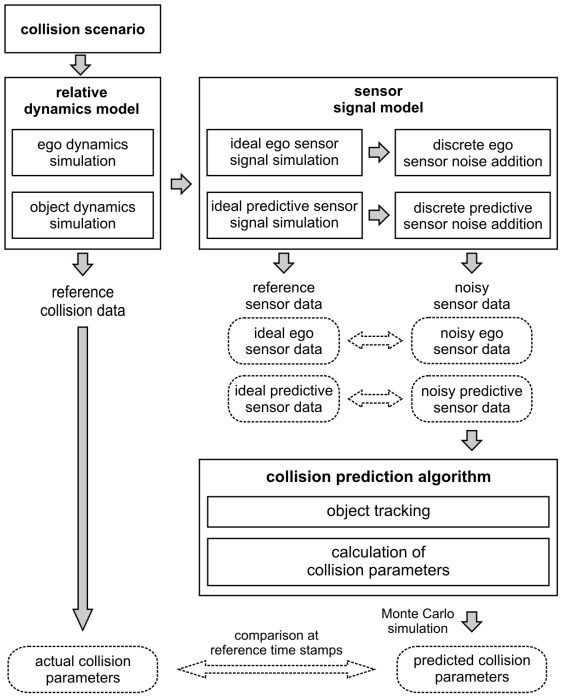

Figure 2. Outline of the paper

Throughout the paper vectors and matrices are denoted by lower and upper case bold letters. A $M \times N$ zero matrix is dented by $\mathbf{0}_{M \times N}$.

MEASUREMENT DATA

In this chapter the model-based generation process of noisy measurements as input data for a collision prediction algorithm is described. Firstly the two-dimensional relative dynamics model used for the simulation of ideal sensor data concerning the ego vehicle and an ego-mounted predictive sensor measuring relative position data is explained. Afterwards the application of sensor noise to the simulated exact reference data is depicted.

Relative dynamics model

For the motion simulation of the ego and opponent vehicle in specific collision scenarios a nonlinear single track model with a Pacejka tire force approach as described in [6] was applied (see Figure 3). This model offers a good two-dimensional description of the global vehicle movement in stationary as well as dynamic driving scenarios disregarding effects of pitch and roll. As only the global vehicle trajectory over ground and not the exact knowledge of internal system state variables such as wheel rota-

tion speeds or forces was of interest the model was regarded as sufficient for this study. In the following, as shown in Figure 3 the capital letters X and Y denote an earth-bound coordinate system, the lower case letters x and y a vehicle-bound coordinate system that is rotated with the yaw angle ψ with respect to the X-axis, and the lower case letters x_v and y_v a vehicle-bound coordinate system that is rotated with the slip angle β with respect to the x-axis. Vectors with the subscripts XY, xy or $x_v y_y$ represent values in the corresponding coordinate systems.

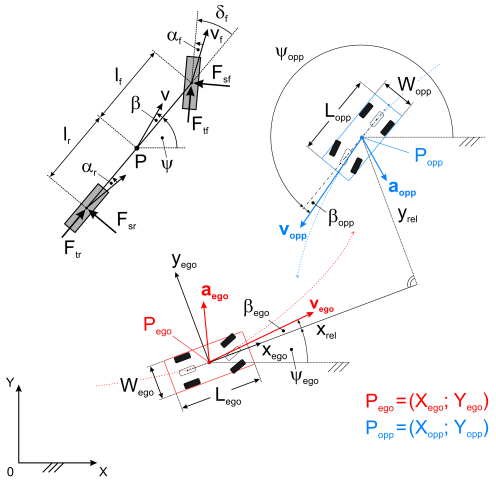

Figure 3. Relative dynamics simulation based on a nonlinear single track model

In the relative dynamics simulation environment the flat projection of each vehicle body was regarded as rectangular and symmetric to the longitudinal axis of the single track model. The basic single track model equations are summarized in the following. The tire slip angles α_f and α_r at the front (subscript f) and rear (subscript r) wheel are given by the subsequent kinematic relations containing the frontal steering angle δ_f, the yaw rate $\dot{\psi}$, the velocity v, the vehicle slip angle β and the center of mass distances l_f from the frontal and l_r from the rear end of the vehicle [7]:

$$\alpha_f = \delta_f - \arctan\left(\frac{l_f \cdot \dot{\psi} + v \cdot \sin\beta}{v \cdot \cos\beta}\right) \tag{1}$$

$$\alpha_r = \arctan\left(\frac{l_r \cdot \dot{\psi} - v \cdot \sin\beta}{v \cdot \cos\beta}\right). \tag{2}$$

The vehicle center of mass acceleration a_{lon} and a_{lat} in longitudinal (x_v) and lateral (y_v) trajectory direction can be calculated on the basis of the principle of linear momentum as a function of δ_f, β, the vehicle mass m as well as the tangential and side tire forces F_t and F_s at the front and rear tire:

$$\mathbf{a} = \begin{bmatrix} a_{lon} \\ a_{lat} \end{bmatrix}_{x_v y_v} = \begin{bmatrix} \dot{v} \\ v \cdot (\dot{\psi} + \dot{\beta}) \end{bmatrix}_{x_v y_v}$$
$$= \begin{bmatrix} \frac{1}{m} \cdot (F_{tr} \cdot \cos\beta + F_{tf} \cdot \cos(\delta_f - \beta) \\ \quad + F_{sr} \cdot \sin\beta - F_{sf} \cdot \sin(\delta_f - \beta)) \\ \frac{1}{m} \cdot (-F_{tr} \cdot \sin\beta + F_{tf} \cdot \sin(\delta_f - \beta) \\ \quad + F_{sr} \cdot \cos\beta + F_{sf} \cdot \cos(\delta_f - \beta)) \end{bmatrix}_{x_v y_v}. \tag{3}$$

The vehicle yaw acceleration $\ddot{\psi}$ results from the principle of conservation of angular momentum depending on the mass moment of inertia I_{zz} around the vehicle z-axis (in a right-hand coordinate system with the origin in the vehicle center of mass P and the x- and y-axis according to Figure 3):

$$\ddot{\psi} = \frac{1}{I_{zz}} \cdot (F_{sf} \cdot \cos\delta_f \cdot l_f + F_{tf} \cdot \sin\delta_f \cdot l_f - F_{sr} \cdot l_r). \tag{4}$$

The temporal change $\dot{\boldsymbol{r}}$ in the global vehicle center of mass position is given by the following kinematic equation:

$$\dot{\mathbf{r}} = \mathbf{v} = \begin{bmatrix} \dot{X} \\ \dot{Y} \end{bmatrix}_{XY} = \begin{bmatrix} v \cdot \cos(\psi + \beta) \\ v \cdot \sin(\psi + \beta) \end{bmatrix}_{XY}. \tag{5}$$

With the Pacejka tire forces given by [7]

$$F_{sf} = C_3 \cdot \sin(C_2 \cdot \arctan(C_1 \cdot \alpha_f - C_4 \cdot (C_1 \cdot \alpha_f - \arctan(C_1 \cdot \alpha_f)))) \tag{6}$$

$$F_{sr} = C_3 \cdot \sin(C_2 \cdot \arctan(C_1 \cdot \alpha_r - C_4 \cdot (C_1 \cdot \alpha_r - \arctan(C_1 \cdot \alpha_r)))) \tag{7}$$

as a function of the constant frontal and rear tire parameters C_{fi} and C_{ri}, with $i \in \{1, 2, 3, 4\}$, and the frontal and rear tire slip angles the presented system of differential equations can be solved by numerical integration. This allows the calculation of the global vehicle center of mass position $\boldsymbol{r}$ in X- and Y-direction as well as the vehicle yaw angle ψ and slip angle β as a function of time and therefore defines the vehicle trajectory over ground.

On the basis of the single track model trajectory ideal sensor data concerning the ego vehicle state is available. For this study it is assumed that in the ego vehicle the absolute ego center of mass speed v_{ego} is known based on wheel speed measurements and the yaw rate $\dot{\psi}_{ego}$ as well as the center of mass acceleration $a_{x_{ego}}$ in x_{ego}-direction and $a_{y_{ego}}$ in y_{ego}-direction are directly measured by body-mounted sensors. The corresponding state variables can be derived from the integrated vehicle

trajectory via the following equations:

$$v_{ego} = |\mathbf{v}_{ego}| = \sqrt{\dot{X}_{ego}^2 + \dot{Y}_{ego}^2} \tag{8}$$

$$\dot{\psi}_{ego} = \frac{d\psi_{ego}}{dt} \tag{9}$$

$$\begin{aligned} a_{x_{ego}} &= \cos(\beta_{ego}) \cdot \dot{v}_{ego} \\ &\quad - \sin(\beta_{ego}) \cdot v_{ego} \cdot (\dot{\psi}_{ego} + \dot{\beta}_{ego}) \end{aligned} \tag{10}$$

$$\begin{aligned} a_{y_{ego}} &= \sin(\beta_{ego}) \cdot \dot{v}_{ego} \\ &\quad + \cos(\beta_{ego}) \cdot v_{ego} \cdot (\dot{\psi}_{ego} + \dot{\beta}_{ego}). \end{aligned} \tag{11}$$

The parallel simulation of two trajectories offers the possibility to calculate the relative position data $\boldsymbol{r}_{P_{opp}/P_{ego}}$ measured by an ideal ego-mounted predictive sensor which can be calculated for any given reference point $\boldsymbol{r}_{P_{opp}}$ on the opponent vehicle.

For a predictive sensor located at $\mathbf{r}_{P_{sens}}$ and mounted at a displacement of $x_{P_{sens}/P_{ego}}$ in x_{ego}-direction and $y_{P_{sens}/P_{ego}}$ in y_{ego}-direction relative to the ego center of mass $\mathbf{r}_{P_{ego}}$ the relative location measurement of the opponent reference point $\mathbf{r}_{P_{opp}}$ is given by:

$$\begin{aligned} &\begin{bmatrix} x_{sens} \\ y_{sens} \end{bmatrix}_{x_{ego}y_{ego}} := \mathbf{r}_{P_{opp}/P_{sens}} = \mathbf{r}_{P_{opp}} - \mathbf{r}_{P_{sens}} = \\ &= \begin{bmatrix} X_{P_{opp}} \\ Y_{P_{opp}} \end{bmatrix}_{XY} - \left[\begin{bmatrix} X_{P_{ego}} \\ Y_{P_{ego}} \end{bmatrix}_{XY} + \begin{bmatrix} x_{P_{sens}/P_{ego}} \\ y_{P_{sens}/P_{ego}} \end{bmatrix}_{x_{ego}y_{ego}} \right] \\ &= \begin{bmatrix} (X_{P_{opp}} - X_{P_{ego}}) \cos\psi_{ego} \\ +(Y_{P_{opp}} - Y_{P_{ego}}) \sin\psi_{ego} - x_{P_{sens}/P_{ego}} \\ -(X_{P_{opp}} - X_{P_{ego}}) \sin\psi_{ego} \\ +(Y_{P_{opp}} - Y_{P_{ego}}) \cos\psi_{ego} - y_{P_{sens}/P_{ego}} \end{bmatrix}_{x_{ego}y_{ego}} \\ &= \begin{bmatrix} x_{rel} - x_{P_{sens}/P_{ego}} \\ y_{rel} - y_{P_{sens}/P_{ego}} \end{bmatrix}_{x_{ego}y_{ego}}. \end{aligned} \tag{12}$$

The relative position data x_{sens} and y_{sens} measured by the predictive ego sensor allows the calculation of the relative center of mass position $\boldsymbol{r}_{rel}$ via the following equation in which $\mathbf{r}_{P_{opp}}$ particularly refers to the opponent center of mass:

$$\begin{aligned} \mathbf{r}_{rel} &= \mathbf{r}_{P_{opp}} - \mathbf{r}_{P_{ego}} = \begin{bmatrix} x_{rel} \\ y_{rel} \end{bmatrix}_{x_{ego}y_{ego}} \\ &= \begin{bmatrix} x_{sens} + x_{P_{sens}/P_{ego}} \\ y_{sens} + y_{P_{sens}/P_{ego}} \end{bmatrix}_{x_{ego}y_{ego}}. \end{aligned} \tag{13}$$

The derived relative center of mass position data over time also allows the determination of the relative velocity $\boldsymbol{v}_{rel}$ between the ego and the opponent center of mass by:

$$\begin{aligned} \mathbf{v}_{rel} &= \mathbf{v}_{P_{opp}} - \mathbf{v}_{P_{ego}} = \dot{\mathbf{r}}_{P_{opp}} - \dot{\mathbf{r}}_{P_{ego}} \\ &= \dot{\mathbf{r}}_{rel} = \begin{bmatrix} \dot{x}_{rel} - \dot{\psi}_{ego} \cdot y_{rel} \\ \dot{y}_{rel} + \dot{\psi}_{ego} \cdot x_{rel} \end{bmatrix}_{x_{ego}y_{ego}}. \end{aligned} \tag{14}$$

The relative acceleration between the two vehicle centers of mass can then be calculated by:

$$\begin{aligned} &\mathbf{a}_{rel} = \mathbf{a}_{P_{opp}} - \mathbf{a}_{P_{ego}} = \dot{\mathbf{v}}_{P_{opp}} - \dot{\mathbf{v}}_{P_{ego}} = \dot{\mathbf{v}}_{rel} = \\ &= \begin{bmatrix} \ddot{x}_{rel} - \ddot{\psi}_{ego} y_{rel} - 2\dot{\psi}_{ego}\dot{y}_{rel} - \dot{\psi}_{ego}^2 x_{rel} \\ \ddot{y}_{rel} + \ddot{\psi}_{ego} x_{rel} + 2\dot{\psi}_{ego}\dot{x}_{rel} - \dot{\psi}_{ego}^2 y_{rel} \end{bmatrix}_{x_{ego}y_{ego}}. \end{aligned} \tag{15}$$

The simulated ideal measurement data concerning the ego vehicle and the relative position data concerning the opponent vehicle measured by a predictive sensor will be used as input for a collision prediction algorithm estimating the expected geometric and kinematic collision parameters after the noise model explained in the following section is applied.

Noise model

In order to model the effect of statistically inexact measurements by real sensors noise is applied both to the ego vehicle data and the predictive sensor data from the relative dynamics simulation. Systematic sensor errors are regarded as compensable and therefore not taken into account. As Gaussian random distributions offer a good means to model measurement scattering the measurement errors are assumed to be normally distributed with a given standard deviation σ around the mean measurement value μ, see Figure 4. As the area of $\pm$ 4σ

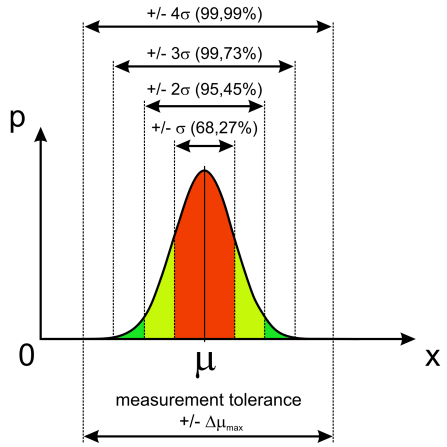

Figure 4. Normal distribution with a given standard deviation

around the mean value μ in a Gaussian normal distribution contains more than 99,99 percent of the noisy measurement values the standard deviation for the applied noise process was defined on the basis of a given measurement tolerance $\pm$ $\Delta\mu_{max}$ via:

$$\sigma := \frac{\Delta\mu_{\max}}{4}. \tag{16}$$

The following equations show the noisy measurements for the ideal ego state variables velocity v_{ego}, yaw rate $\dot{\psi}_{ego}$ and the accelerations $a_{x_{ego}}$ and $a_{y_{ego}}$:

$$v_{ego}^{noisy} = v_{ego} + \eta_{v_{ego}}(0, \sigma_{v_{ego}}) \quad (17)$$
$$a_{x_{ego}}^{noisy} = a_{x_{ego}} + \eta_{a_{x_{ego}}}(0, \sigma_{a_{x_{ego}}}) \quad (18)$$
$$a_{y_{ego}}^{noisy} = a_{y_{ego}} + \eta_{a_{y_{ego}}}(0, \sigma_{a_{y_{ego}}}) \quad (19)$$
$$\dot{\psi}_{ego}^{noisy} = \dot{\psi}_{ego} + \eta_{\dot{\psi}_{ego}}(0, \sigma_{\dot{\psi}_{ego}}), \quad (20)$$

where $\eta(\mu, \sigma)$ denotes a Gaussian random variable with mean μ and variance σ^2.

The noisy measurements for the ideal predictive sensor data x_{rel} and y_{rel} as well as for the ideally detected opponent length W_{sens} are given by:

$$x_{sens}^{noisy} = x_{sens} + \eta_{x_{sens}}(0, \sigma_{x_{sens}}) \quad (21)$$
$$y_{sens}^{noisy} = y_{sens} + \eta_{y_{sens}}(0, \sigma_{y_{sens}}) \quad (22)$$
$$W_{sens}^{noisy} = W_{sens} + \eta_{W_{sens}}(0, \sigma_{W_{sens}}). \quad (23)$$

Figure 5 shows an example for ideal and discrete noisy measurement data over time.

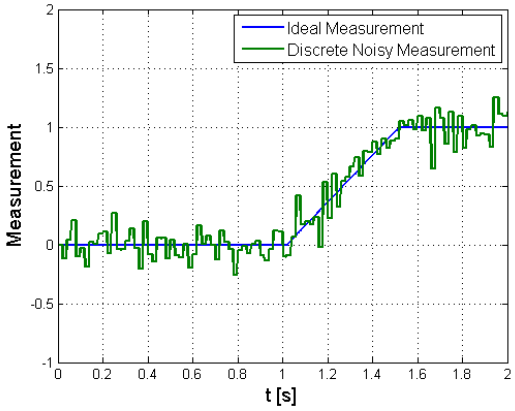

Figure 5. Ideal and discrete noisy measurement data over time

For the further analysis steps the standard deviation of the noisy ego measurements was regarded as constant over time (assumed values for σ see Table 1).

Table 1.
Assumed standard deviations for ego sensor noise

sensor	σ
v_{ego}	0.075 m/s
$a_{x_{ego}}$	0.050 m/s2
$a_{y_{ego}}$	0.050 m/s2
$\dot{\psi}_{ego}$	0.005 rad/s

For the predictive sensor measurements (x_{sens}, y_{sens} and W_{sens}) a more complex model was applied. The standard deviation σ of the applied measurement noise was modeled as distance dependent via the following linear equation because the maximum resolution of the sensor element limits the detection accuracy in a decreasing manner along the measurement distance:

$$\sigma(d) = \sigma_0 \cdot (1 + c_d \cdot d). \quad (24)$$

The measurement distance d was calculated on the basis of the ideal sensor values x_{sens} and y_{sens}:

$$d = \sqrt{x_{sens}^2 + y_{sens}^2}. \quad (25)$$

The assumed basic standard deviations σ_0 for the predictive sensor are shown in Table 2.

Table 2.
Assumed basic standard deviations for predictive sensor noise

sensor value	σ
x_{sens}	0.125 m
y_{sens}	0.0625 m
W_{sens}	0.075 m

As mentioned in the introduction four predictive sensor variants are used for the Monte Carlo analysis in this paper. The variants differ in terms of σ_0 and c_d as depicted in Table 3.

Table 3.
Analyzed predictive sensor variants

sensor variant	σ_0	c_d
1	σ	0.05 1/m
2	σ	0.10 1/m
3	$2 \cdot \sigma$	0.05 1/m
4	$2 \cdot \sigma$	0.10 1/m

The distance dependent standard deviation scaling factor is illustrated in Figure 6.

COLLISION PREDICTION ALGORITHM

Tracking Model

In order to estimate the position and the velocity of an object—as in common predictive sensors—the discrete state-space formulation

$$\mathbf{x}[k] = f(\mathbf{x}[k-1], \boldsymbol{\eta}[k], \mathbf{u}[k]) \quad (26)$$
$$\mathbf{y}[k] = h(\mathbf{x}[k], \mathbf{w}[k]) \quad (27)$$

is used, with $\mathbf{x}[k]$ being the state vector at the time instance indexed by k, $\boldsymbol{\eta}$ the system noise, $\mathbf{u}$ the

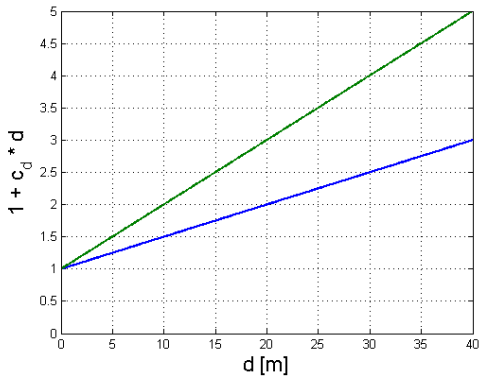

Figure 6. Distance dependent standard deviation scaling of the measurement noise

control vector, $\mathbf{y}$ the measurement vector, $\mathbf{w}$ the measurement noise, and f and h denote the mappings describing the dynamic model and the sensor model. In order to use the well-known notation [8] from (27)—unlike in the rest of the paper—a position vector $[\mathsf{x}, \mathsf{y}]^{\mathrm{T}}$ is notated as $\boldsymbol{r} = [\mathsf{r}_x, \mathsf{r}_y]^{\mathrm{T}}$ in this section. The coordinate system used in the following is a right-hand coordinate system that has its origin in the center of gravity of the ego car and the x-axis points to the front. Since the ego car is moving over ground also the location of the origin of the coordinate system is fixed only for one sample time T and then it is updated. Figure 7 visualizes the movement of the ego car and an object between two time stamps. The coordinate system at time $t_0 - T$,

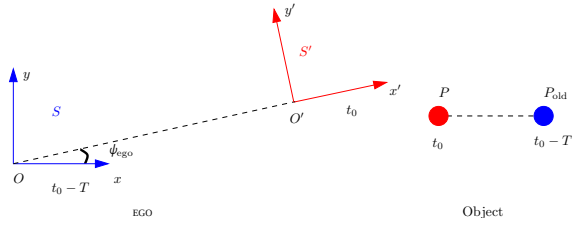

Figure 7. Movement of ego car and object in a sample interval T

having the index $k-1$, is denoted with S, its origin with O and the coordinate system at time instance t_0 with S' and its origin with O'. During the time T the coordinate system rotates with the yaw angle ψ_{ego} and the object moves from the point P_{old} to the point P. In the following the time instance t_0 has the index k. Since the sensor type that is in the focus of this paper measures only positions but additionally also the velocities of the objects in the environment of the car are important, the following state vector will be used

$$\mathbf{x}[k] = \left[\mathsf{r}_{x,S'}^{O'P}[k], \mathsf{r}_{y,S'}^{O'P}[k], \mathsf{v}_{x,S'}^{OP}[k], \mathsf{v}_{y,S'}^{OP}[k]\right]^{\mathrm{T}}, \quad (28)$$

where $\mathsf{r}_{x,S'}^{O'P}[k]$ is the relative distance in x-direction between the object and the ego car at time instance t_0 expressed in the coordinate system S', $\mathsf{r}_{y,S'}^{O'P}[k]$ the relative distance in y-direction, $\mathsf{v}_{x,S'}^{OP}[k]$ and $\mathsf{v}_{x,S'}^{OP}[k]$ the components of the velocity vector over ground but rotated in the coordinate system S'. The advantages of implementing the tracking using the velocity over ground instead of the relative velocity are described in [9].

To find a suitable model for the mapping h in the dynamic equation (26) firstly the position and then the velocity of ego car and object must be expressed in S' based on the values in the coordinate system S.

The position $[\mathsf{r}_{x,S}^{OO'}[k], \mathsf{r}_{y,S}^{OO'}[k]]^{\mathrm{T}}$ of the ego car at t_0 expressed in the cooridinate system S is

$$\mathsf{r}_{x,S}^{OO'}[k] = \mathsf{v}_{x,S}^{O}[k-1]T + \eta_{\mathsf{a}_{x,S}^{O}} \frac{T^2}{2} \quad (29)$$

$$\mathsf{r}_{y,S}^{OO'}[k] = \mathsf{v}_{y,S}^{O}[k-1]T + \eta_{\mathsf{a}_{y,S}^{O}} \frac{T^2}{2}, \quad (30)$$

with $\mathsf{v}_{x,S}^{O}[k-1]$ and $\mathsf{v}_{y,S}^{O}[k-1]$ being the vector components of the velocity over ground rotated in the coordinate system S, and $\eta_{\mathsf{a}_{x,S}^{O}}$ and $\eta_{\mathsf{a}_{y,S}^{O}}$ representing noise terms which take into account that during an time interval T the acceleration of the car is neglected.

The position $[\mathsf{r}_{x,S}^{OP}[k], \mathsf{r}_{y,S}^{OP}[k]]^{\mathrm{T}}$ of the object at time instance t_0 expressed in the coordinate system S is

$$\mathsf{r}_{x,S}^{OP}[k] = \mathsf{r}_{x,S}^{OP_{\mathrm{old}}}[k-1] + \mathsf{v}_{x,S}^{OP_{\mathrm{old}}}[k-1]T + \eta_{\mathsf{a}_{x,S}^{OP_{\mathrm{old}}}} \frac{T^2}{2} \quad (31)$$

$$\mathsf{r}_{y,S}^{OP}[k] = \mathsf{r}_{y,S}^{OP_{\mathrm{old}}}[k-1] + \mathsf{v}_{y,S}^{OP_{\mathrm{old}}}[k-1]T + \eta_{\mathsf{a}_{y,S}^{OP_{\mathrm{old}}}} \frac{T^2}{2}, \quad (32)$$

where $[\mathsf{r}_{x,S}^{OP_{\mathrm{old}}}[k-1], \mathsf{r}_{y,S}^{OP_{\mathrm{old}}}[k-1]]^{\mathrm{T}}$ is the position of the object at time $t_0 - T$ expressed in S, $[\mathsf{v}_{x,S}^{OP_{\mathrm{old}}}[k-1], \mathsf{v}_{y,S}^{OP_{\mathrm{old}}}[k-1]]^{\mathrm{T}}$ the components of the object's velocity vector over ground at time $t_0 - T$ expressed in S, and $\eta_{\mathsf{a}_{x,S}^{OP_{\mathrm{old}}}}$ and $\eta_{\mathsf{a}_{y,S}^{OP_{\mathrm{old}}}}$ noise terms taking into account that the acceleration of the object during a sample interval T is neglected.

With equations (29), (30), (31), and (32) the relative position $[\mathsf{r}_{x,S}^{O'P}[k], \mathsf{r}_{y,S}^{O'P}[k]]^{\mathrm{T}}$ between ego car and object at time instance t_0 expressed in S can be computed as

$$\begin{aligned}\mathsf{r}_{x,S}^{O'P}[k] &= \mathsf{r}_{x,S}^{OP}[k] - \mathsf{r}_{x,S}^{OO'}[k] \\ &= \mathsf{r}_{x,S}^{OP_{\mathrm{old}}}[k-1] + \mathsf{v}_{x,S}^{OP_{\mathrm{old}}}[k-1]T + \eta_{\mathsf{a}_{x,S}^{OP_{\mathrm{old}}}} \frac{T^2}{2} \\ &\quad - \mathsf{v}_{x,S}^{O}[k-1]T - \eta_{\mathsf{a}_{x,S}^{O}} \frac{T^2}{2} \end{aligned} \quad (33)$$

$$\begin{aligned}\mathsf{r}_{y,S}^{O'P}[k] &= \mathsf{r}_{y,S}^{OP}[k] - \mathsf{r}_{y,S}^{OO'}[k] \\ &= \mathsf{r}_{y,S}^{OP_{\text{old}}}[k-1] + \mathsf{v}_{y,S}^{OP_{\text{old}}}[k-1]T + \eta_{\mathsf{a}_{y,S}^{OP_{\text{old}}}} \frac{T^2}{2} \\ &\quad - \mathsf{v}_{y,S}^{O}[k-1]T - \eta_{\mathsf{a}_{y,S}^{O}} \frac{T^2}{2}. \end{aligned} \tag{34}$$

To express the relative distances $\mathsf{r}_{x,S'}^{O'P}[k]$ and $\mathsf{r}_{y,S'}^{O'P}[k]$ in the state vector $\mathbf{x}[k]$ a transformation to S' is necessary, i. e., a rotation with the yaw angle $\psi_{\text{ego}}[k]$:

$$\mathsf{r}_{x,S'}^{O'P}[k] = \cos(\psi_{\text{ego}}[k])\mathsf{r}_{x,S}^{O'P}[k] + \sin(\psi_{\text{ego}}[k])\mathsf{r}_{y,S}^{O'P}[k] \tag{35}$$

$$\mathsf{r}_{y,S'}^{O'P}[k] = cos(\psi_{\text{ego}}[k])\mathsf{r}_{y,S}^{O'P}[k] - \sin(\psi_{\text{ego}}[k])\mathsf{r}_{x,S}^{O'P}[k]. \tag{36}$$

The velocity of the object over ground but rotated into the coordinate system S is

$$\mathsf{v}_{x,S}^{OP}[k] = \mathsf{v}_{x,S}^{OP_{\text{old}}}[k-1] + \eta_{\mathsf{a}_{x,S}^{OP_{\text{old}}}} T \tag{37}$$

$$\mathsf{v}_{y,S}^{OP}[k] = \mathsf{v}_{y,S}^{OP_{\text{old}}}[k-1] + \eta_{\mathsf{a}_{y,S}^{OP_{\text{old}}}} T. \tag{38}$$

In order to express the velocity of the object over ground at time instance t_0 in S' a rotation with $\psi_{\text{ego}}[k]$ must be performed

$$\mathsf{v}_{x,S'}^{OP}[k] = \cos(\psi_{\text{ego}}[k])\mathsf{v}_{x,S}^{OP}[k] + \sin(\psi_{\text{ego}}[k])\mathsf{v}_{y,S}^{OP}[k] \tag{39}$$

$$\mathsf{v}_{y,S'}^{OP}[k] = \cos(\psi_{\text{ego}}[k])\mathsf{v}_{y,S}^{OP}[k] - \sin(\psi_{\text{ego}}[k])\mathsf{v}_{x,S}^{OP}[k]. \tag{40}$$

All relations required to express the mapping h in (26) are now given by (33), (34), (35), (36), (37), (38), (39) and (40). Since only the yaw rate is measurable in cars, the yaw rate is approximated by $\psi_{\text{ego}}[k] = \dot{\psi}_{\text{ego}}[k] \cdot T$. Also it is assumed that the sampling interval T is small so that the noise terms $\eta_{\mathsf{a}_{x,S}^{O}}$ and $\eta_{\mathsf{a}_{y,S}^{O}}$ corresponding the the ego car can be neglected in (33) and (34). The following vectors and matrices are introduced to find an expression for h that can be used in a Kalman filter

$$\tilde{\mathbf{R}}[k] = \begin{bmatrix} \cos(\dot{\psi}_{\text{ego}}[k]T) & \sin(\dot{\psi}_{\text{ego}}[k]T) \\ -\sin(\dot{\psi}_{\text{ego}}[k]T) & \cos(\dot{\psi}_{\text{ego}}[k]T) \end{bmatrix},$$

$$\mathbf{R}[k] = \begin{bmatrix} \tilde{\mathbf{R}}[k] & \mathbf{0}_{2\times 2} \\ \mathbf{0}_{2\times 2} & \tilde{\mathbf{R}}[k] \end{bmatrix}, \; \tilde{\boldsymbol{F}} = \begin{bmatrix} 1 & 0 & T & 0 \\ 0 & 1 & 0 & T \\ 0 & 0 & 1 & 0 \\ 0 & 0 & 0 & 1 \end{bmatrix},$$

$$\tilde{\boldsymbol{G}} = \begin{bmatrix} T^2/2 & 0 \\ 0 & T^2/2 \\ T & 0 \\ 0 & T \end{bmatrix}, \; \mathbf{x}[k-1] = \begin{bmatrix} \mathsf{r}_{x,S'}^{O'P_{\text{old}}}[k-1] \\ \mathsf{r}_{y,S'}^{O'P_{\text{old}}}[k-1] \\ \mathsf{v}_{x,S'}^{OP_{\text{old}}}[k-1] \\ \mathsf{v}_{y,S'}^{OP_{\text{old}}}[k-1] \end{bmatrix}$$

$$\boldsymbol{\eta}[k] = \begin{bmatrix} \eta_{\mathsf{a}_{x,S}^{OP_{\text{old}}}} \\ \eta_{\mathsf{a}_{y,S}^{OP_{\text{old}}}} \end{bmatrix}, \tilde{\mathbf{u}}[k] = \begin{bmatrix} -\mathsf{v}_{x,S}^{O}[k-1]T \\ 0 \\ 0 \\ 0 \end{bmatrix}.$$

The second component in $\tilde{\mathbf{u}}[k]$ is zero since $\mathsf{v}_{y,S}^{O}[k-1] = 0$. Now the dynamic equation (26) can be written as

$$\mathbf{x}[k] = \boldsymbol{F}[k]\mathbf{x}[k-1] + \mathbf{u}[k] + \boldsymbol{G}[k]\boldsymbol{\eta}[k], \tag{41}$$

with

$$\boldsymbol{F}[k] = \mathbf{R}[k]\tilde{\boldsymbol{F}}, \; \mathbf{u}[k] = \mathbf{R}[k]\tilde{\mathbf{u}}[k], \text{ and } \boldsymbol{G}[k] = \mathbf{R}[k]\tilde{\boldsymbol{G}}. \tag{42}$$

Since the sensor type that is considered in this paper measures only the relative position the measurement vector is $\mathbf{y}[k] = \left[\mathsf{r}_{x,S'}^{O'P}[k], \mathsf{r}_{y,S'}^{O'P}[k]\right]^{\mathrm{T}}$ and (27) can be expressed as

$$\mathbf{y}[k] = \begin{bmatrix} 1 & 0 & 0 & 0 \\ 0 & 1 & 0 & 0 \end{bmatrix} \mathbf{x}[k] + \mathbf{w}[k] = \boldsymbol{H}\mathbf{x}[k] + \mathbf{w}[k]. \tag{43}$$

With the dynamic equation (41) and the measurement equation (43) it is straightforward to apply a Kalman filter [8] in order to estimate the state vector $\mathbf{x}[k]$.

Computation of collision parameters

A collision prediction algorithm has to anticipate the prospective motion of the ego vehicle and surrounding objects on the basis of realistic movement assumptions and estimate the expected collision parameters under the given premises. The prediction may both depend on kinematic ego state data and relative object measurement data provided by a predictive sensor mounted on the moving ego vehicle. The prediction process is necessary because a predictive sensor is usually not able to measure the geometric and kinematic impact conditions in adequate precision right before the collision. This results from limitations in the sensor field of view as well as the necessary time interval for the object creation and the movement tracking algorithms.

For an online estimation of the collision effect in the ego vehicle the geometric and kinematic initial conditions of the impact have to be described explicitly by the predicted collision parameters. Therefore the following parameters defining the relative position and movement of the ego and opponent bounding boxes at the time of collision were selected, see Figure 8.

The relative geometric and kinematic movement state of the two vehicle bounding boxes is described

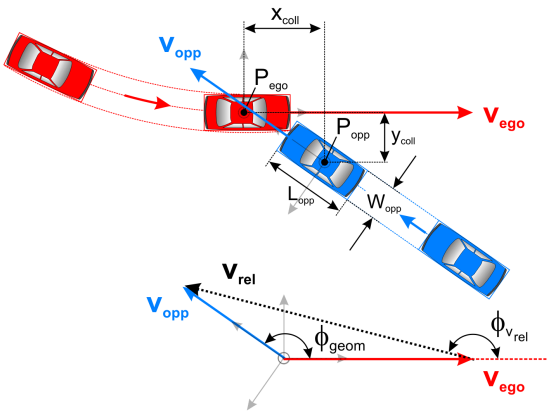

Figure 8. Predicted collision parameters as initial conditions of the mechanical impact

by the relative reference point position x_{coll} in x_{ego}-direction and y_{coll} in y_{ego}-direction as well as the geometric angle ϕ_{geom} between the vehicle longitudinal axes (in Figure 8 the slip angles of both vehicles are chosen negligibly small) in combination with the ego width W_{ego}, the ego length L_{ego}, the opponent width W_{opp} and the opponent length L_{opp}. As a real predictive sensor will mostly not be able to detect the complete opponent length the parameter L_{opp} may also refer to the current length of the detected part of the opponent vehicle. The impact direction is specified by the angle $\phi_{v_{rel}}$ between the relative velocity vector and the ego velocity vector as well as the absolute value v_{rel} of the relative velocity vector. Furthermore the expected time to collision (TTC) is estimated on the basis of the underlying assumptions. For this study the collision parameters were calculated on the basis of a no change assumption concerning the current movement state of the ego vehicle and the opponent in two dimensions over ground. The assumption no change extrapolates the actual moving state of the ego vehicle and the opponent sensor object on the basis of a Taylor series for kinematic state variables. The closer the collision comes the better the no change assumption is able to predict values that fit the real development of the accident scenario.

The ego and object trajectories are calculated on the basis of the following correlations concerning the predicted movement state at t_0 defined by the velocity v, the yaw angle ψ and the slip angle β along the prediction time t_{pred}:

$$\begin{aligned} v(t_{pred}) &= v(t_0) + \frac{dv}{dt}(t_0) \cdot t_{pred} \\ &\quad + \frac{1}{2} \cdot \frac{d^2v}{dt^2}(t_0) \cdot t_{pred}^2 + ... \\ &\approx v(t_0) + \frac{dv}{dt}(t_0) \cdot t_{pred} \end{aligned} \tag{44}$$

$$\begin{aligned} \psi(t_{pred}) &= \psi(t_0) + \frac{d\psi}{dt}(t_0) \cdot t_{pred} \\ &\quad + \frac{1}{2} \cdot \frac{d^2\psi}{dt^2}(t_0) \cdot t_{pred}^2 + ... \\ &\approx \psi(t_0) + \frac{d\psi}{dt}(t_0) \cdot t_{pred} \end{aligned} \tag{45}$$

$$\begin{aligned} \beta(t_{pred}) &= \beta(t_0) + \frac{d\beta}{dt}(t_0) \cdot t_{pred} \\ &\quad + \frac{1}{2} \cdot \frac{d^2\beta}{dt^2}(t_0) \cdot t_{pred}^2 + ... \\ &\approx \beta(t_0) + \frac{d\beta}{dt}(t_0) \cdot t_{pred}. \end{aligned} \tag{46}$$

On the basis of the movement state variable approximations at each prediction time step the vehicle velocity vector $\boldsymbol{v}$ can be calculated by:

$$\mathbf{v}\,(t_{pred}) = \begin{bmatrix} v(t_{pred}) \cdot \cos(\psi(t_{pred}) + \beta(t_{pred})) \\ v(t_{pred}) \cdot \sin(\psi(t_{pred}) + \beta(t_{pred})) \end{bmatrix}_{xy}. \tag{47}$$

The absolute vehicle position $\boldsymbol{r}$ along the predicted trajectory can then be calculated by integration:

$$\mathbf{r}\,(t_{pred}) = \int_{t_0}^{t_{pred}} v(\tilde{t}_{pred}) \cdot d\tilde{t}_{pred} = \begin{bmatrix} x(t_{pred}) \\ y(t_{pred}) \end{bmatrix}_{xy}. \tag{48}$$

The absolute acceleration $\boldsymbol{a}$ along the trajectory is given by:

$$\begin{aligned} \mathbf{a}(t_{pred}) &= \frac{d}{dt_{pred}}\mathbf{v}(t_{pred}) = \\ &= \begin{bmatrix} \dot{v}(t_{pred}) \\ v(t_{pred}) \cdot (\dot{\psi}(t_{pred}) + \dot{\beta}(t_{pred})) \end{bmatrix}_{x_v y_v} \\ &= \begin{bmatrix} a_{lon}(t_{pred}) \\ a_{lat}(t_{pred}) \end{bmatrix}_{x_v y_v}. \end{aligned} \tag{49}$$

The resulting trajectory on the basis of a given and numerically extrapolated working point of the ego vehicle movement is shown in the Figure 9. In this case the ego slip angle β_{ego} is assumed to be known with a diminishing slip rate $\dot{\beta}_{ego}$ so that it remains constant during the prediction. Both the ego vehicle state as well as the opponent vehicle movement are predicted on the basis of the described no change trajectory extrapolation, see Figure 10. Whereas for the ego vehicle the acceleration, yaw rate and the slip angle are assumed to be known for the opponent vehicle detected by the predictive sensor only the velocity in x_{ego}- and y_{ego}-direction is used for the prediction but not its acceleration, yaw or slip rate. This assumption is

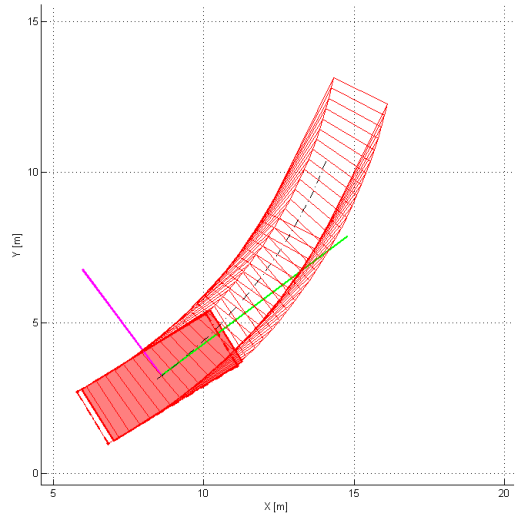

Figure 9. No change prediction on the basis of the current moving state

based on the fact that these variables are very hard to estimate with a sensor only directly measuring the position and not the relative velocity. Furthermore a diminishing slip angle is supposed for the opponent vehicle which is a good approximation for stable driving maneuvers considering the increasing number of ESP systems limiting the slip angle in modern vehicles. The resulting collision parame-

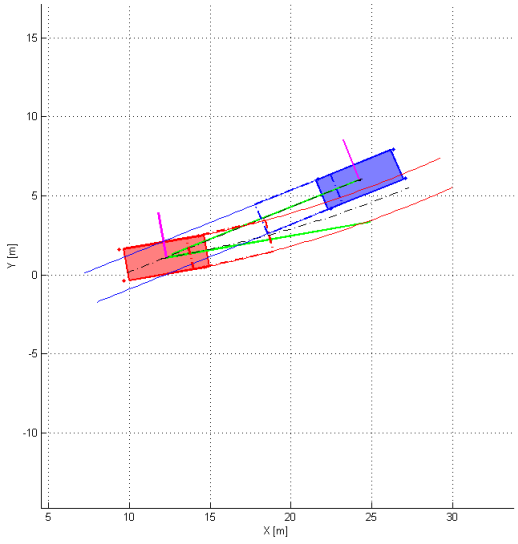

Figure 10. No change prediction of the expected collision constellation and parameters

ters described above are calculated on the basis of an analysis concerning the overlap of two rectangular bounding boxes around the vehicle contours at each point of the prediction time along the trajectories. Therefore the precision of the TTC-prediction is limited by the integration time interval during the discrete prediction process. The smaller the prediction time interval is selected the more exact the kinematic and geometric collision parameters can be calculated.

MONTE CARLO SIMULATION

On the basis of the described measurement data generation and the collision prediction algorithm Monte Carlo simulations were performed to analyze the effect of the noisy measurement input data on the predicted collision parameters in three selected car2car-collision scenarios.

Simulation scenarios and process

In the following three critical traffic situations each resulting in a car2car-collision are presented. The scenarios will be analyzed concerning the sensitivity of the predicted collision parameters on the basis of noisy input data in this chapter. The accident scenarios are illustrated in Figures 11, 12, and 13.

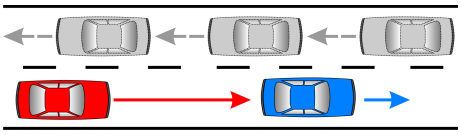

Figure 11. Scenario 1: straight rear-end collision with full overlap

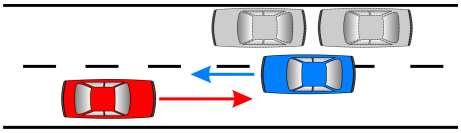

Figure 12. Scenario 2: straight frontal collision with partial overlap

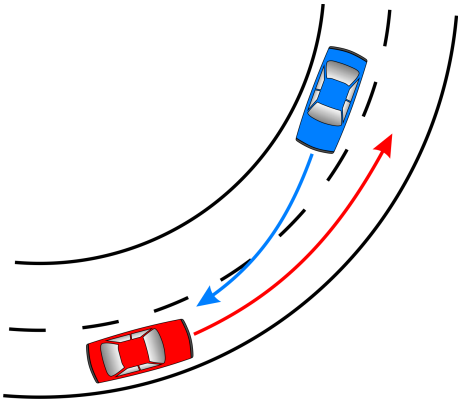

Figure 13. Scenario 3: curved frontal collision with partial overlap

In the first scenario the ego vehicle driving at a speed of 50 km/h hits the back of an opponent vehicle at a velocity of 10 km/h with full overlap. The second scenario represents a straight frontal impact

with an overlap of 40 percent within which the ego vehicle at a velocity of 50 km/h collides with the opponent vehicle driving at a speed of 40 km/h. In the last scenario the opponent vehicle driving at 57.4 km/h leaves its lane on a curved road segment and collides frontally with the oncoming ego vehicle with a velocity of 56.2 km/h. For simplicity concerning the further analysis steps the selected scenarios are all stationary concerning velocities, yaw and slip rates. Of course dynamic scenarios with sudden break or steering inputs can also be evaluated with the proposed method. For the simulation process both vehicles are assumed to be equally dimensioned with a length of 5 m and a width of 2 m.

For the sensitivity analysis of the collision parameter calculation on the basis of the Monte Carlo method for each collision scenario 1000 simulation runs were performed with MATLAB/Simulink [10] at a sample time of 1 ms for a sufficiently exact dynamics simulation. In each scenario Gaussian noise with the assumed standard deviation (see Chapter "Noise Model") was added to the ideal measurements at a discrete measurement sample time of 20 ms modeling the processing cycle for ego and predictive sensor data. For every scenario two reference time stamps in relation to the actual time of collision (TOC) at TOC - 400 ms and TOC - 100 ms were selected. The reference collision parameters were calculated on the basis of the ideal dynamics data. At every reference time step of a scenario the predicted collision parameters on the basis of the noisy input values for the collision prediction module as well as the corresponding reference values were logged. The resulting differences between the prediction outputs and the reference values were analyzed concerning the statistical mean and standard deviation as well as the minimum and maximum values. The input values for the collision prediction module at each time step over all the 1000 simulation runs per scenario were all normally distributed with the given (distance dependent) standard deviation around the nominal value and a noise value limitation to the $\pm\, 4\sigma$ interval. The simuation runs were performed with constant ego sensor noise parameters and the four predictive sensor noise variations according to section "Noise model".

Simulation results

In the following the results of the Monte Carlo simulation process are illustrated. For each of the three simulated collision scenarios introduced in the last section the noisy predictive sensor data as input for the collision prediction module as well as the resulting differences ΔTTC, Δv_{rel}, $\Delta \phi_{v_{rel}}$, $\Delta \phi_{geom}$, Δx_{coll} and Δy_{coll} between the prediction outputs and the reference values are presented for two reference points of time (TOC - 400 ms and TOC - 100 ms). The noisy ego vehicle sensor data is only illustrated for scenario 1 at TOC - 400 ms, see Figure 14, because each of the four ego sensor signals was disturbed with a Gaussian noise of constant standard deviation over all scenarios and reference points of time. The generated plots show the mean, minimum and maximum values (continuous lines, left y-axis) as well as the standard deviation (dashed line, right y-axis) at the regarded reference point of time for the four analyzed sensor variants (concerning all performed simulation runs under the given sensor noise). Figure 14 illustrates

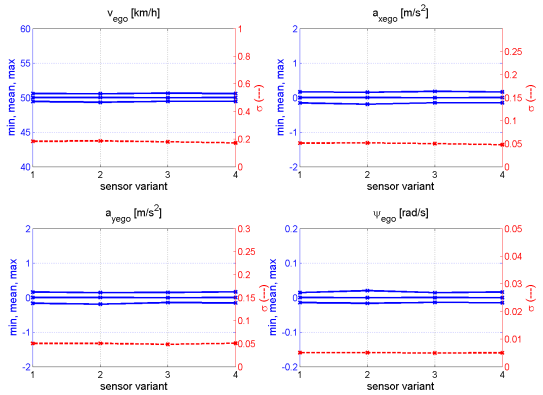

Figure 14. Scenario 1: Noisy ego sensor signals at TOC - 400 ms

the ego sensor data values in scenario 1 at TOC - 400 ms for the four presented (predictive) sensor variants in scenario 1. As the ego sensor data values were disturbed with constant noise parameters the mean, minimum and maximum sensor values over all the four sensor variants at TOC - 400 ms approximately remain constant with the chosen standard deviation. In this scenario the measured ego speed v_{ego} varies in an interval of about $\pm$ 1 km/h around the nominal value of 50 km/h, the acceleration measurements $a_{x_{ego}}$ and $a_{y_{ego}}$ in an interval of approximately $\pm$ 0.2 m/s^2 and the yaw rate $\dot{\psi}_{ego}$ in a range of about $\pm$ 0.02 rad/s. The effect of the distance dependent predictive sensor noise over the four variants at TOC - 400 ms in scenario 1 is shown in Figure 15. The standard deviation at that reference point of time increases from sensor variant 1 to sensor variant 4 along with the interval between the maximum and minimum values of the measured relative position x_{rel} in x_{ego}- and y_{rel} in y_{ego}-direction and the opponent width W. TOC - 400 ms is related to a mean x_{rel}-value of about 9 m and a mean y_{rel}-value of 0 m concerning the rear-end collision. The predicted collision parameters at TOC - 400 ms in scenario 1 scatter as a result of the given noisy input, see Figure 16. The differ-

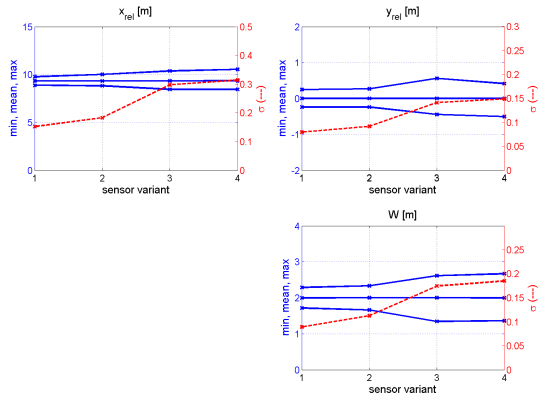

Figure 15. Scenario 1: Noisy predictive sensor signals at TOC - 400 ms

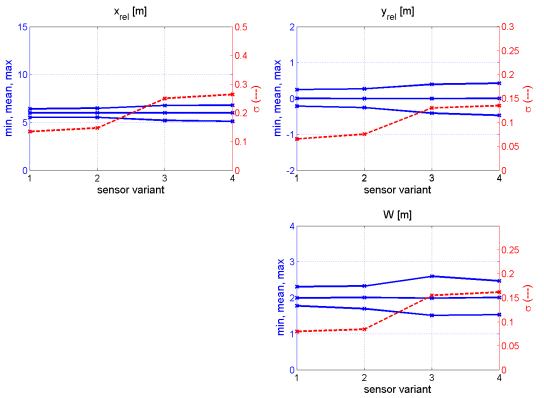

Figure 17. Scenario 1: Noisy predictive sensor signals at TOC - 100 ms

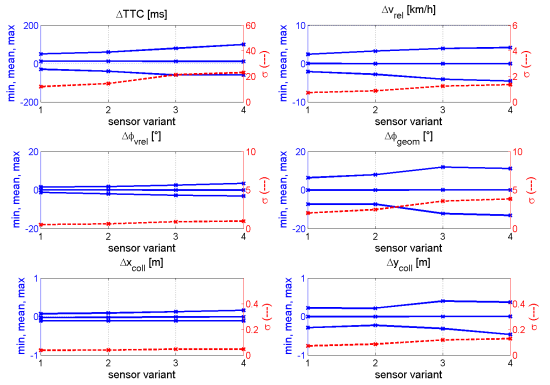

Figure 16. Scenario 1: Predicted collision parameters at TOC - 400 ms

ence between the predicted and the reference value varies between a resulting minimum and maximum value for each collision parameter. In this case for every parameter the difference increases along with the sensor variant. The predicted TTC varies in an interval smaller than ± 100 ms around the reference value for all the considered sensor variants. The mean ΔTTC-value is not exactly 0 ms because of the prediction tolerance due to the discrete prediction time interval of 10 ms. The relative velocity v_{rel} was predicted with a tolerance better than ± 5 km/h decreasing from sensor variant 4 down to 1. The predicted geometric collision angle ϕ_{geom} is more diffuse than the relative velocity angle $\phi_{v_{rel}}$. Both parameters were estimated with an accuracy better than ± 14° concerning the reference in all sensor variants. The predicted relative collision location parameter x_{coll} only varies in a quite small range of about ± 0.2 m. The predicted lateral collision opponent location y_{coll} scatters in a wider range of up to approximately ± 0.5 m. At the examined point of time the accuracy of the prediction decreases from sensor variant 1 to sensor variant 4 for all collision parameters. At TOC - 100 ms in scenario 1 the predicted TTC varies in a decreased interval of about ± 50 ms around the reference value in all sensor variants based on smaller predictive input parameter variations, see Figures 17 and 18. The relative velocity v_{rel} is predicted with an accuracy of approximately ± 4 km/h. As seen above the predicted relative velocity angle $\phi_{v_{rel}}$ again doesn't scatter as much as the geometric collision angle ϕ_{geom}. Both parameters remain in an interval smaller than about ± 12° over all sensor variants. The relative collision location is predicted relatively exact in x_{ego}-direction (± 0.20 m) and doesn't exceed an interval of ± 0.25 m in y_{ego}-direction. As a result of the decreasing predictive sensor input noise at TOC - 100 ms compared to TOC - 400 ms the collision parameters are estimated with a better (or at least identical) accuracy for all sensor variants.

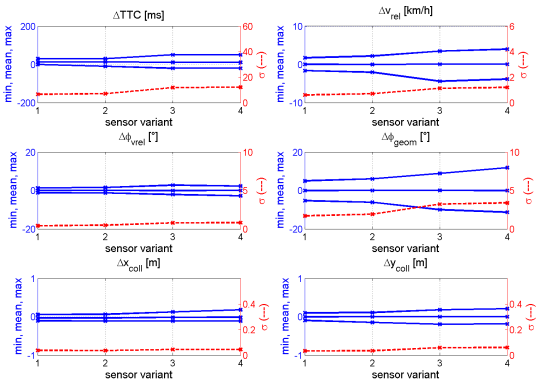

Figure 18. Scenario 1: Predicted collision parameters at TOC - 100 ms

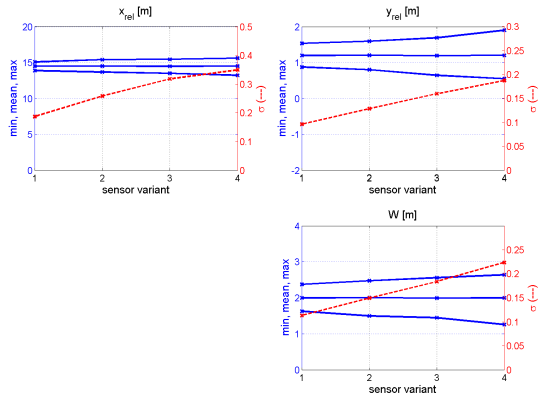

Figure 19. Scenario 2: Noisy predictive sensor signals at TOC - 400 ms

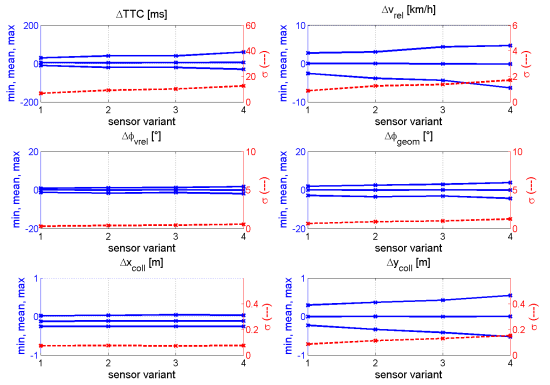

Figure 20. Scenario 2: Predicted collision parameters at TOC - 400 ms

In scenario 2 at TOC - 400 ms, see Figures 19 and 20, the predicted TTC varies in a maximum interval of about ± 60 ms around the reference value in an increasing manner along the predictive sensor variant due to the growing sensor noise at that point of time. The relative velocity v_{rel} is predicted with a minimum accuracy of approximately ± 6 km/h. Again the predicted relative velocity angle $\phi_{v_{rel}}$ doesn't vary as much as the geometric collision angle ϕ_{geom}. Both parameters remain in an interval smaller than about ± 5° over all sensor variants. The relative collision location x_{coll} is predicted in a range of about ± 0.3 m in x_{ego}-direction and doesn't exceed an interval of ± 0.6 m in y_{ego}-direction. At TOC - 100 ms in scenario 2 the TTC variation interval decreases to approximately ± 20 ms due to the significantly smaller predictive sensor noise, see Figures 21 and 22. Whereas the prediction scatter intervals for the relative velocity v_{rel}, the geometric angle ϕ_{geom}, the relative velocity angle $\phi_{v_{rel}}$ and the x_{coll}-location parameter do not change significantly compared to the values at

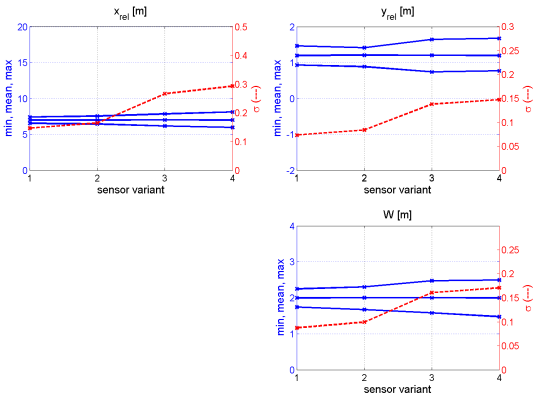

Figure 21. Scenario 2: Noisy predictive sensor signals at TOC - 100 ms

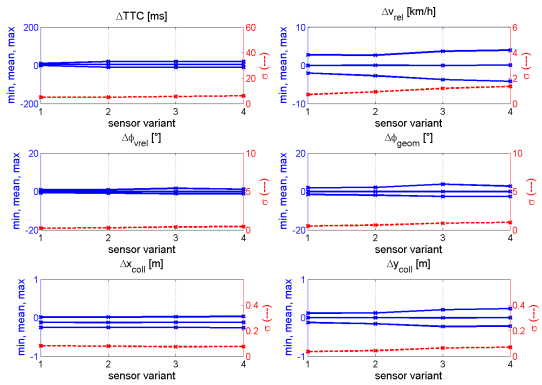

Figure 22. Scenario 2: Predicted collision parameters at TOC - 100 ms

TOC - 400 ms, the prediction of the y_{coll}-parameter gets significantly better. This results both from the less scattering y_{rel}-values at TOC - 100 ms as well as the decreasing effect of errors in the movement prediction direction with a decreasing distance.

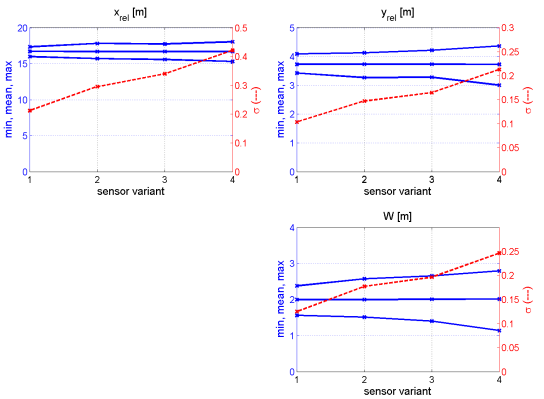

Figure 23. Scenario 3: Noisy predictive sensor signals at TOC - 400 ms

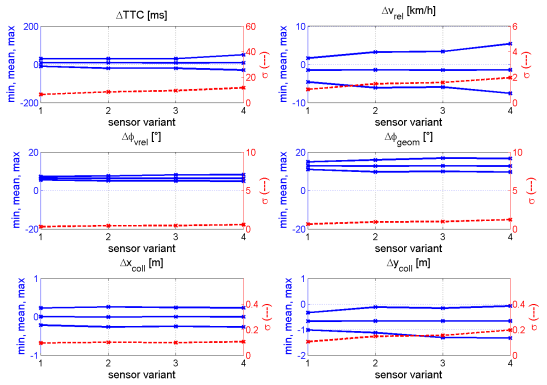

Figure 24. Scenario 3: Predicted collision parameters at TOC - 400 ms

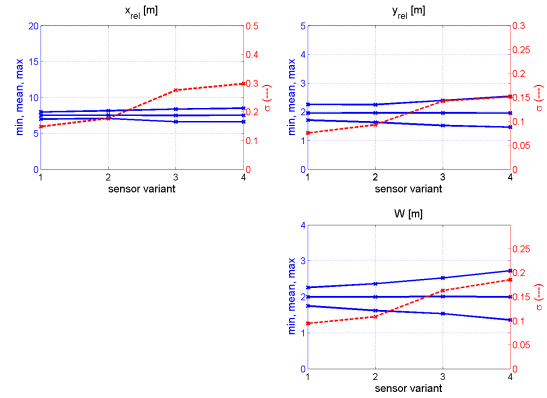

Figure 25. Scenario 3: Noisy predictive sensor signals at TOC - 100 ms

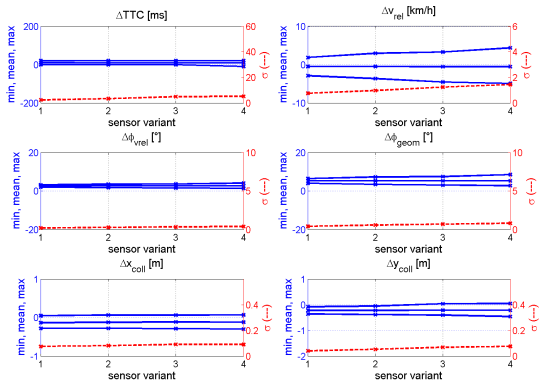

Figure 26. Scenario 3: Predicted collision parameters at TOC - 100 ms

In collision scenario 3 the predictive measurement scattering monotonically increases over all sensor variants at each reference point of time and decreases from TOC - 400 ms to TOC - 100 ms, see Figures 23 to 26. As both vehicle trajectories are curved and the yaw and slip rate of the opponent vehicle are not estimated in the collision prediction module the no change prediction assumes a straight opponent trajectory that doesn't take into account the lateral opponent vehicle movement. This results in a visible difference of the mean prediction values for the relative velocity v_{rel} and the collision angles $\phi_{v_{rel}}$ and ϕ_{geom} as well as the lateral collision location y_{coll} in y_{ego}-direction from the reference values. The depicted difference between the mean values for the predicted collision angles and the y_{coll}-location parameter gets smaller from TOC - 400 ms to TOC - 100 ms because the effect of the inexact movement assumption decreases with a smaller distance. In this case the inexact collision parameter prediction is not only influenced by the measurement value scattering but also by the inexact movement assumption in the opponent trajectory generation. The measurement scattering effects on the predicted collision parameters are similar to those observed in scenarios 1 and 2.

CONCLUSIONS

The optimization of passive safety applications by the use of predictive sensor data requires a sufficiently exact prediction of collision parameters characterizing the type and severity of a collision. Ego vehicle state sensors as well as predictive sensors only measure with a given tolerance and resolution so that predicted geometric and kinematic collision parameters always scatter depending on the characteristics of the applied sensors as well as the sensor signal processing steps. In this paper a method for the model-based evaluation of sensor noise effects on the predicted collision parameters along the whole signal processing chain with a predictive sensor able to measure distances but not velocities was presented. On the basis of the developed method a study on the effects of measurement scattering concerning the predicted collision parameters was accomplished. Therefore fixed noise parameters for the ego vehicle sensors and two different basic noise levels for the predictive sensor combined with two noise dependencies along the measurement distance were assumed. Their effects on the collision parameter prediction were analyzed in three selected collision scenarios. Whereas in the straight collision scenarios the mean values of the predicted collision parameters based on noisy input data fitted the reference values very accurately in curved scenarios the collision prediction algorithm assuming a straight trajectory for the opponent vehicle (as opponent yaw rates are very hard to estimate) resulted in a time-dependent mean value in the geometric parameter prediction. Depending on the sensor noise parameters the geometric

collision parameters in all analyzed scenarios scattered in a specific range representing the accuracy of the prediction under the given premises. For the three analyzed scenarios under the made assumptions the TTC prediction scattering at TOC - 400 ms and TOC - 100 ms didn't exceed a range of ± 100 ms around the reference value, the relative velocity angle prediction was always in an interval of ± 9° and the predicted geometric angle varied in a maximum interval of ± 18°. The relative reference point position in longitudinal ego vehicle body direction scattered in a range of ± 0.30 m at most and the relative reference point position in lateral ego body direction differed in a maximum range of ± 0.60 m (at TOC - 400 ms) respectively ± 0.25 m (at TOC - 100 ms) in straight scenarios and in a range from -0.10 m to -1.30 m (at TOC - 400 ms) respectively -0.50 m to 0.10 m (at TOC - 100 ms) in the curved scenario. The results show the challenge of collision predictions in the case of small vehicle overlaps and in curved scenarios. For the reliable detection and prediction of the collision parameters in these scenarios the sensor noise parameters have to be kept low in combination with an adequate dynamic object tracking with ego-compensation even in areas close to the ego vehicle. The effect of dynamic scenarios with sudden steering or brake inputs concerning the parameter prediction was not yet analyzed and has to be observed in future studies.

REFERENCES

[1] Eichberger, A., Wallner, D., Hirschberg, W. 2009. "A situation based method to adapt the vehicle restraint system in frontal crashes to the accident scenario." Proceedings of the 21st ESV Conference; International Conference on the Enhanced Safety of Vehicles, 2009.

[2] Moritz, R. 2000. "Pre-crash sensing - functional evolution based on short range radar sensor platform." SAE Technical Paper Series, 00IBECD-11, 2000.

[3] Skutek, M., Linzmeier, D.T., Appenrodt, N., Wanielik, G. 2005. "A precrash system based on sensor data fusion of laser scanner and short range radars." IEEE 8th International Conference on Information Fusion, 2005.

[4] Gietelink, O., Ploeg, J., De Schutter, B., Verhaegen, M. 2006. "Development of advanced driver assistance systems with vehicle hardware-in-the-loop simulations." Technical report, Delft University of Technology, 2006.

[5] Pudenz, K. 2010. "Der Audi A7 Sportback: Sicherheitssysteme." ATZonline, July 2010.

[6] Karrenberg, S. 2008. "Zur Erkennung unvermeidbarer Kollisionen von Kraftfahrzeugen mit Hilfe von Stellvertretertrajektorien." Technical report, Technische Universität Carolo-Wilhelmina zu Braunschweig, 2008.

[7] Mitschke, M., Wallentowitz, H. 2004. "Dynamik der Kraftfahrzeuge." Springer, 2004.

[8] Bar-Shalom, Y., Li, X. R., Kirubarajan, T. 2001. "Estimation with Applications to Tracking and Navigation." John Wiley & Sons, July 2001.

[9] Altendorfer, R. 2009. "Observable dynamics and coordinate systems for automotive target tracking." IEEE Intelligent Vehicles Symposium, 2009.

[10] MATLAB 2009b, Copyright © 1984-2009 The MathWorks Inc.